Simulation of the Taylor impact test and analysis of damage evolution using a nucleation and growth based approach

L. Campagne-Lambert, Loïc Daridon, Omar Oussouaddi, Saïd Ahzi, X. Sun

Simulation of the Taylor impact test and analysis of damage evolution using a nucleation and growth based approach

L. Campagne[1], L. Daridon[2], O. Oussouaddi[3], S. Ahzi[4] and X. Sun[5]

[1]GIP-InSIC, 27 Rue d'Hellieule, Saint-Dié-des-Vosges, 88100, France

[2]LMGC-UMR CNRS 5508, University Montpellier II-CC 048, Montpellier, 34095, France

[3]EMMS, Department of Physics, FST, University Moulay Ismaïl, Errachidia, Morocco

[4]IMFS-UMR 7507, University Louis Pasteur, 2 Rue Boussingault, Strasbourg, 67000, France

[5]Pacific Northwest National Laboratory, Richland, WA 99352, USA

Abstract

Computational modeling of the Taylor impact test, using OFHC copper rods are carried out for two impact velocities ($260m/s$ and $365m/s$). The aim of this work is to demonstrate the efficiency of the recently proposed material model for dynamic plasticity and failure for metals. This model combines the use of a damage approach based on void nucleation and growth, with the Mechanical Threshold Stress (MTS) model for the evolution of the flow stress in isotropic plasticity. The proposed approach is implemented in the finite element code ABAQUS/Explicit via a user material subroutine and the symmetric Taylor impact test, using copper rods, is simulated. The predicted results are compared to the experimental results reported in the open literature and good agreement is found for both shape change and damage distribution.

Keywords: Taylor Impact, high strain rates, viscoplasticity, void nucleation, void growth, finite element.

1. Introduction

In 1948, Taylor [1], Whiffen [2] and Carrington and Gayler [3] conducted series of tests to determine the dynamic yield stress of materials deformed at very high strain rates. For the last 60 years, many studies have been carried out around this test. During the 1980s and 1990s, Taylor impact experiments were performed to study the material mechanical properties under dynamic loading at high strain rates in the range of 10^4- $10^5 s^{-1}$ [4-8]. Recently, work on Taylor impact (Experiment and modelling) has been reported by numerous investigators; for instance Addessio et

al. [9], Maudlin et al. [10], Rule and Jones [11] among many others. In 1999, House et al. [12] showed how the high-speed photography can be used to approximate the strain rate and the stress-strain curves for the tested material. This study can give additional information on the constitutive properties of material under high strain rate conditions. In 2003, an experimental investigation was reported by Wang et al. [13] to study the influence of porosity on the dynamic yield stress of porous metals under high loading rates.

The classic Taylor impact consists of impacting (using a gas gun) a cylindrical rod of the material being tested against an infinitely rigid target [1]. The symmetric version of the Taylor impact test is achieved by impacting a stationary target rod with an initial radius, R_{init}, and an identical flyer rod as shown in Figure 1. The impactor and target have an initial cross-sectional area $A_0 = \pi R_{init}^2$ with respectively initial length, L_{I0}, L_{T0}, and an initial material density ρ_0. Figure 1b shows the final stage of deformation where L_{IF}, L_{TF}, X_I and X_T denote the length of the entire deformed and the undeformed section of the impactor and target, respectively.

The strain rate and temperature dependency become particularly important at high strain rate where adiabatic plastic flow may produce significant temperature changes in the material. Several constitutive models have been developed to describe the material deformation behaviour as a function of strain-rate and temperature under dynamic loading. Some of these models are based on dislocations overcoming obstacles through thermal activation as in the Mechanical Threshold Stress (MTS) model [14] and the Zerilli-Armstrong model [5] and the model of Molinari and Ravichandran [15]. Others models are based on phenomenological approach such as the model of Molinari and Clifton [16], Klopp et al. [17] and the Johnson-Cook [4] model. The material failure under high strain rate can be divided into two categories: dynamic fracture and dynamic shear localization. We are interested in the case of dynamic failure by fracture involving nucleation, growth, and coalescence of voids or cracks. These mechanisms of failure in polycrystalline materials are often dislocation controlled. Most of the existing failure models are based on phenomenological approaches rather than mechanistic approaches. Reviews of these models can be found in the literature (see for instance Hanim and Ahzi [18]). Several mechanistic-based (void nucleation and growth) approaches for dynamic failure were proposed in the literature. In the works of Tuler and Butcher [19], Gilman [20] an empirical law was proposed to predict spall damage. However, the works of Curran et al. [21], Rajendran et al. [22] and Addessio et al. [9] are based on mechanistic approaches considering void nucleation and growth.

In this paper, we make use of the recently proposed model by Campagne et al. [23] for dynamic plasticity and failure in metals to simulate the flow behaviour and damage evolution in OFHC

copper rods under symmetric Taylor impact test. The simulations are carried out by implementing the proposed constitutive laws in the commercial finite element code ABAQUS/Explicit [24] via a user material subroutine VUMAT. The proposed modelling approach combines the MTS model for the flow stress with a model for spherical void nucleation and growth under high strain rates. This model accounts only for a weak coupling between damage and the stress-strain response since it allows the evolved damage to degrade the elastic properties only. The results obtained can therefore be considered as a first approximation. The obtained results from the proposed mechanistic approach are compared to the ones computed using the phenomenological model of Johnson-Cook [4] and the experimental result of Addessio et al. [9].

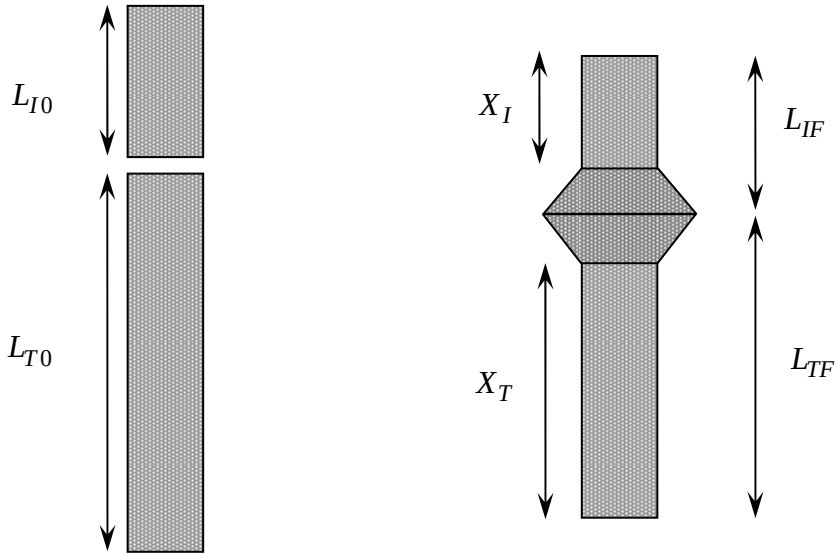

[a] Initial state [b] Final state

Figure 1. Schematic of the symmetrical Taylor impact test

2. Viscoplasticity and damage evolution modeling

2.1 Viscoplasticity model

To describe the flow stress evolution, we use the MTS model proposed by Follansbee and Kocks [14]. This model is based on the physics of dislocation motion. It takes into account the dislocation motion by introducing an internal state variable called "Mechanical Threshold Stress": $\hat{\sigma}$. This internal state variable is a function of two components: an athermal stress $\hat{\sigma}_a$ and a thermally activated stress $\hat{\sigma}_t$ due to dislocation interaction. Based on this assumption, Follansbee and Kocks [14] derived the following expression for the flow stress σ_y:

$$\sigma_y = \hat{\sigma}_a + \hat{\sigma}_t S\left(\dot{\varepsilon}_{eq}^p, T\right) = \hat{\sigma}_a + \left(\hat{\sigma} - \hat{\sigma}_a\right)\left(1 - \left[\frac{kT\left(\frac{\dot{\varepsilon}_0}{\dot{\varepsilon}_{eq}^p}\right)}{g_0 G_{eff} b^3}\right]^{\frac{1}{q}}\right)^{\frac{1}{p}} \quad (1)$$

where G_{eff} is the effective shear modulus (defined in paragraph 2.2), k is the Boltzmann constant, T is the temperature, b is the Burger's vector, $\dot{\varepsilon}_{eq}$ is the equivalent plastic strain rate, $\dot{\varepsilon}_0$ is a reference strain rate, g_0 is the normalized activation energy, and p and q are the constants that characterize the shape of the energy barrier (obstacle) profile. The scaling factor S depends on strain rate and temperature.

The hardening rate, θ for OFHC copper which takes into account the dislocation accumulation and the dynamic recovery, is expressed by the following relation:

$$\theta = \frac{d\hat{\sigma}}{d\varepsilon_{eq}^p} = \theta_0\left(1 - F(X)\right) \quad \text{with} \quad F(X) = \frac{tanh(2X)}{tanh(2)} \quad and\ X = \frac{\hat{\sigma} - \hat{\sigma}_a}{\hat{\sigma}_s - \hat{\sigma}_a} \quad (2)$$

where θ_0 is an experimentally determined stage II strain-hardening rate and $\hat{\sigma}_s$ is the saturation stress, given by the following expression:

$$ln\left(\frac{\dot{\varepsilon}_{S0}}{\dot{\varepsilon}_{eq}^p}\right) = -\frac{Gb^3 g_{0\varepsilon S}}{kT} ln\left(\frac{\hat{\sigma}_S}{\hat{\sigma}_{S0}}\right) \quad (3)$$

Here, $\dot{\varepsilon}_{s0}$ is the saturation strain rate at $0K$, $\hat{\sigma}_{s0}$ describes the saturation threshold stress for the deformation at $0K$ and $g_{0\varepsilon s}$ is a normalized activation energy for dislocation-dislocation interaction.

The MTS model accounts for the softening due to the adiabatic heating through the update of the temperature T during the high strain rate deformation. In this case, the temperature rise ΔT is given by:

$$\Delta T = \frac{\chi}{\rho C_p} \int \sigma_{ij} d\varepsilon_{ij}^p \quad (4)$$

where σ_{ij} are the Cauchy stress tensor components, $d\varepsilon_{ij}^{p}$ are the increment of plastic strain tensor components, χ is the fraction of plastic work converted to heat, ρ is the density and C_p is the specific heat. The parameters of the MTS model used in our finite element simulations and the material data for OFHC copper rods are given in Table 1 and Table 2 [14].

Material parameters	OFHC copper
Normalized activation energy g_0	1.6
p	$2/3$
q	1
Stress at $0K$ σ_{s0} [MPa]	900
Saturation strain rate at 0 K $\dot{\varepsilon}_{s0}$ [s^{-1}]	10^7
Initial strain hardening rate θ_0 [MPa]	2315
Athermal stress σ_a [MPa]	40

Table1**.** MTS-Model parameters (for OFHC) [14]

Material data	OFHC copper
Specific heat C_p [J/kgK]	385
Taylor-Quinney's coefficient χ	0.9
Poisson's coefficient ν	0.351
Young Modulus E [GPa]	127.72
Density ρ_0 [kg/m^3]	8960
Melting temperature T_m [K]	1356
k/b^3 [MPa/K]	0.823
Shear modulus [GPa]	47.27

Table2. Material properties for OFHC copper [14]

2.2 Damage evolution and failure criterion

In order to model damage evolution, we proposed to use a mechanistic model [23]. This approach, associated with the MTS model for plasticity, is based on void nucleation and growth (NAG). As we are interested in high strain rates loading where the damage can quickly reach its

critical value for failure due to the rapid void growth, void coalescence process can therefore be neglected.

In the following, we briefly address the constitutive equations used for the damage model since the details can be found in the work of Campagne et al. [23]. The material porosity factor f is determined from the total relative void volume V_T and given by:

$$f = \frac{V_T}{1+V_T} \tag{5}$$

where V_T can be expressed as the sum of relative volumes due to preexisting, nucleation and growth of voids:

$$V_T = V_I + \int_0^t \left(\dot{V}_{N\varepsilon} + \dot{V}_{N\sigma} \right) dt + V_G \tag{6}$$

in which, V_I, is the initially relative void volume, V_G is the relative void volume produced by growth, $\dot{V}_{N\varepsilon}$ and $\dot{V}_{N\sigma}$ are the relative void volume rates due to nucleation controlled by strain and stress respectively.

$$V_I = 8\pi N_I R_0^3 \tag{7}$$

where R_0 is a nucleation size parameter, which is assumed to be the same for preexisting and nucleated voids. The term N_I is the number per unit volume of preexisting voids.

The nucleated void volume rate controlled by strain is given by:

$$\dot{V}_{N\varepsilon} = 8\pi R_0^3 \dot{N}_\varepsilon \qquad \text{where} \quad \dot{N}_\varepsilon = \dot{N}_0 \left[1 - exp\left(-\omega t \frac{\dot{\gamma}}{\dot{\gamma}_0} \right) \right] \tag{8}$$

where ω is a frequency factor and $\dot{N}_0$ is a material constant which represents the density of nucleation sites per unit time (which can be determined as the density of nucleation sites N_0 divided by the incubation time). Also, $\dot{\gamma}$ and $\dot{\gamma}_0$ are the shear strain rate and reference shear strain rate, respectively.

The nucleated void volume rate controlled by stress is given by:

$$\dot{V}_{N\sigma} = 8\pi R_0^3 \dot{N}_\sigma \qquad \text{where} \quad \begin{cases} \dot{N}_\sigma = \dot{N}_0 \, exp\left(\dfrac{P_s - P_{N0}}{P_1} \right) & if \;\; P_s \rangle P_{N0} \\ \dot{N}_\sigma = 0 & if \;\; P_s \le P_{N0} \end{cases} \tag{9}$$

where P_s is the tensile pressure, P_{N0} the nucleation threshold pressure and P_1 is a reference pressure

Therefore, the relative nucleation void volume, $V_{N\varepsilon}$, controlled by strain is given by:

$$V_{N\varepsilon} = \int_0^t \dot{V}_{N\varepsilon} dt = 8\pi R_0^3 \int_0^t \dot{N}_0 \left[1 - exp\left(-\omega t \left(\frac{\dot{\gamma}}{\dot{\gamma}_0} \right) \right) \right] dt = 8\pi R_0^3 N_\varepsilon \tag{10}$$

And, the relative nucleation void volume, $V_{N\sigma}$, controlled by pressure is given by:

$$V_{N\sigma} = \int_0^t \dot{V}_{N\sigma} dt = 8\pi R_0^3 \int_0^t \dot{N}_0 \, exp\left(\frac{\langle Ps - P_{N0} \rangle^+}{P_1} \right) dt = 8\pi R_0^3 N_\sigma \tag{11}$$

where $\langle P_s - P_{N0} \rangle^+$ designates the positive part of $P_s - P_{N0}$.

The tensile pressure P_S is defined from the equation of state. Here, we use the Mie-Grüneisen equation [25]:

$$P_s = C' \left(\frac{\rho_s}{\rho_0} - 1 \right) + \Gamma \rho_s E_I \tag{12}$$

where C' is the bulk modulus ($C' = \rho_0 C_0^2$), Γ is the Grüneisen coefficient, E_I the internal energy, ρ_s the current density and ρ_0 the initial density.

The nucleated microscopic voids will subsequently grow if the applied stress exceeds the growth threshold stress, σ_{g0}. The growth equation for the radius of a void is expressed as follow [23]:

$$R = R_0 \, exp\left(\frac{h\pi(1-\upsilon)}{16 g^2 G_{eff}^2 t^*} \int_0^t \left(\langle \sigma_m - \sigma_{g0} \rangle^+ \right)^2 dt \right) \tag{13}$$

In equation (13), $\langle \sigma_m \text{-} \sigma_{g0} \rangle^+$ designates the positive part of $\sigma_m \text{-} \sigma_{g0}$. To grow, the void should have nucleated (or preexisted) and the mean stress σ_m should exceed the growth threshold stress σ_{g0}. The parameter h can be approximated by $h = 3$ [26]. g is a constant, which is representative of the type of the growth process [26].

To perform the simulation of planar impact, the loading cycle t^* is evaluated by the shock theory [27]. The initial duration of the peak shock pulse in an impact is approximately equal to twice the

travel time of the shock wave through the projectile. Thus, to determine the loading cycle t^*, we use the following approximate expression:

$$t^* = \frac{2d_0}{U_S} \tag{14}$$

where d_0 is the thickness of the projectile and the linear shock velocity U_s is defined by the linear Hugoniot form:

$$U_S = C_0 + sU_P \tag{15}$$

where C_0 is the velocity of the elastic wave, s is an empirical parameter available in the literature for many materials [28] and U_p is the particle velocity.

The velocity of the elastic wave is defined by the following expression:

$$C_0 = \left(\frac{E(1-\upsilon)}{\rho_0 (1+\upsilon)(1-2\upsilon)} \right)^{\frac{1}{2}} \tag{16}$$

We have recently proposed this NAG model and used it to predict dynamic failure in different shock problems using the finite element code ABAQUS/Explicit: spalling in planar impact including two geometries are considered, Taylor impact, perforation [29] and to simulate the blanking process of thin copper sheets [30].

Based on the relationship for size distribution proposed by Curran et al. [21], the relative void volume through growth is obtained by integration over the entire distribution (Eq. 13). The relative volume produced by growth V_G arises from the growth of both nucleated and existing voids, and it can be described by the following equation:

$$V_G = 8\pi R_0^3 \left[N_I + N_\varepsilon + N_\sigma \right] \left[exp\left(\frac{3h\pi(1-\nu)}{16 g^2 G_{eff}^2 t^*} \int_0^t \left(\left\langle \sigma_{mean} - \sigma_{g0} \right\rangle^+ \right)^2 dt \right) - 1 \right] \tag{17}$$

Using Eq. (17), (10) and (7), equation (6) becomes:

$$V_T = 8\pi R_0^3 \left[N_I + N_\varepsilon + N_\sigma \right] exp\left(\frac{3h\pi(1-\upsilon)}{16 g^2 {G_{eff}}^2 t^*} \int_0^t \left(\left\langle \sigma_m - \sigma_{g0} \right\rangle^+ \right)^2 dt \right) \tag{18}$$

The creation of cavities inside a material domain modifies the mechanical properties of this domain. A damage parameter d is introduced so that the elastic modulus and shear modulus are reduced with increasing damage.

We introduce the notion of effective elastic modulus to account for damage effects on the elastic properties during loading. The effective Young modulus E_{eff} and shear modulus G_{eff} are thus given by:

$$\begin{cases} E_{eff} = E(1-d) & \text{and} \quad G_{eff} = G(1-d) \quad \text{in tensile loading} \\ E_{eff} = E & \text{and} \quad G_{eff} = G(1-d) \quad \text{in compressive loading} \end{cases} \tag{19}$$

where, E and G are their corresponding initial (undamaged) values. In all of the previous equations, the elastic moduli are updated according to (19). The porosity f is determined from the total relative void volume V_T (Eq. 5).

The failure criterion is based on a critical porosity f_C which can be expressed as follows:

$$\begin{aligned} f < f_c &\Rightarrow \text{Damage} \\ f = f_c &\Rightarrow \text{Failure} \end{aligned} \tag{20}$$

The damage parameter *d* can be derived, as function of the effective porosity f^***,** from a self-consistent approach [31]:

$$d = \frac{15(1-\upsilon)}{7-5\upsilon} f^* \tag{21}$$

Here, isotropy is assumed and the porosity factor f is assumed to be uniformly distributed. The effective porosity f^* is defined such that damage initiates at threshold porosity f_t, and that failure occurs when d reaches a critical value d_c corresponding to the critical porosity f_c. The damage evolution in ductile metals begins after a threshold strain [32-33] associated in our case to threshold porosity f_t. The effective porosity f^* is defined by the following relation [23]:

$$\begin{cases} f^* = 0 & \text{if} \quad f \in [0, f_t] \\ f^* = f_c \left(\dfrac{f - f_t}{f_c - f_t} \right) & \text{if} \quad f \in [f_t, f_c] \\ f^* = f_c & \text{if} \quad f \geq f_c \end{cases} \tag{22}$$

This model is implemented in the Finite Element Code ABAQUS/Explicit [24] via a user material subroutine (VUMAT). The material parameters for the mechanistic damage model are given in Table 3. Their values lay in a physically acceptable range defined by Curran et al. [21] and Weertman [26].

Material parameters data	OFHC copper
Nucleation void radius R_0 [m]	10^{-6}
Initial Nucleation rate $\dot{N}_0$ [$Nb/m^3.s$]	10^{22}
Initial number of voids	10^{10}
Frequency ω [s^{-1}]	10^6
g	0.329
Hydrostatic threshold stress σ_{g0} [MPa]	500
Nucleation threshold stress P_{N0} [GPa]	1.95
Mie-Grüneisen coefficient Γ	2
Critical relative void volume V_c (critical porosity f_c)	0.5 (0.33)
Empirical parameter s	1.49
Elastic wave velocity C_0 [m/s]	3940

Table3. Material parameters for the proposed mechanistic model for damage evolution and for failure in OFHC copper [29]

3. The Johnson-Cook model

We recall here the basic equations of the dynamic plasticity model of Johnson-Cook [4] expresses the evolution of the phenomenological flow stress as a function of the strain, strain rate and temperature. The flow stress is given by multiplicative effects:

$$\sigma_y = \left(A + B\varepsilon^n\right)\left(1 + C\,ln\frac{\dot{\varepsilon}}{\dot{\varepsilon}_0}\right)\left(1 - \left[\frac{T - T_r}{T_m - T_r}\right]^m\right) \tag{23}$$

where A, B, C, n and m are material parameters, $\dot{\varepsilon}$ is the strain rate, $\dot{\varepsilon}_0$ is a reference strain rate which is usually taken equal 1 s^{-1}, T_r is a reference temperature and T_m is the melting temperature.

This model is purely phenomenological and does not take into account any history effect. This model is widely used in basic studies of dynamic plasticity problems and has the advantage of being already implemented in commercial finite elements codes such as ABAQUS. However, the strong coupling between damage evolution and flow stress evolution is not considered.

The corresponding tensile failure criterion of Johnson-Cook, which is already implemented in the commercial finite elements code ABAQUS [24], is given by:

$$\sigma_{mean} = \sigma_c \tag{24}$$

The material parameters for the phenomenological approach are given in Table 4.

Parameters	OFHC copper
Yields stress σ_0 [MPa]	90
B [MPa]	292
C	0.025
n	0.31
m	1.09
$\dot{\varepsilon}_0$	1
Reference temperature T_r [K]	300

Table4. Parameters data for the Johnson-Cook model for OFHC copper [34]

4. Application to dynamic failure during the Taylor impact test

In Taylor impact test, a radial relief wave is generated at the lateral surface of the target. At high projectile velocities, when the decompression wave reaches the centerline (symmetry axis in figure 2) of the target (decompression waves collide) results in a region of tension in which the magnitude of the tensile wave can be sufficiently high to produce a damaged zone along the center line of the impacted specimen (figure 2). Furthermore, a plasticized zone appears in the impacted region (figure 2).

In this simulation, rod on rod impact with the same geometries is considered in the work of Addessio et al. [9]. The projectile and target materials are OFHC copper of cylindrical shapes and their respective dimensions and boundaries are shown in figure 3.

In this study, the predicted results with two approaches are compared: a physical approach considering the "Mechanical Threshold Stress" model associated with the NAG damage model and

a phenomenological approach considering the dynamic plasticity model of Johnson-Cook associated with corresponding tensile rupture criterion described previously. Table 5 summarises the predicted separation time of the projectile from the target for an impact velocity of $260m/s$.

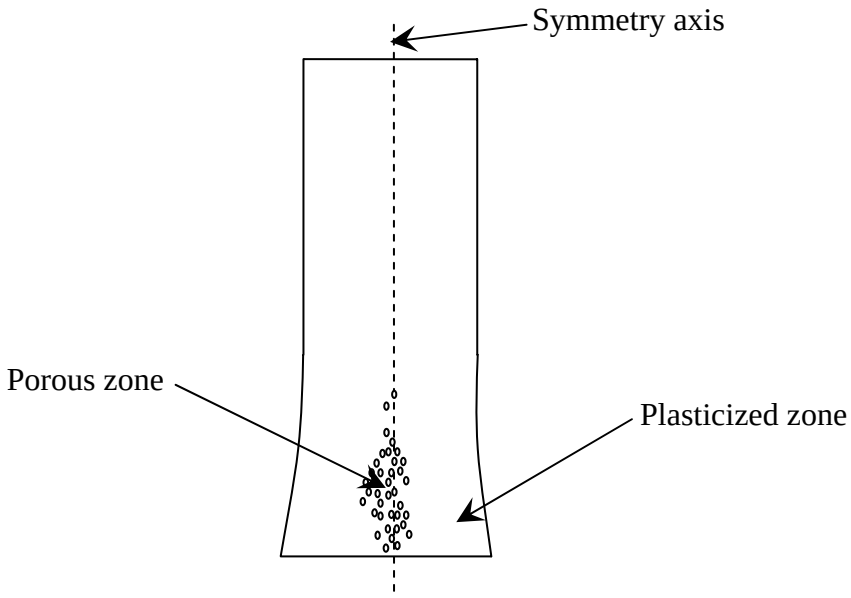

Figure 2. Schematic of the cylinder profile and porosity contour after the impact

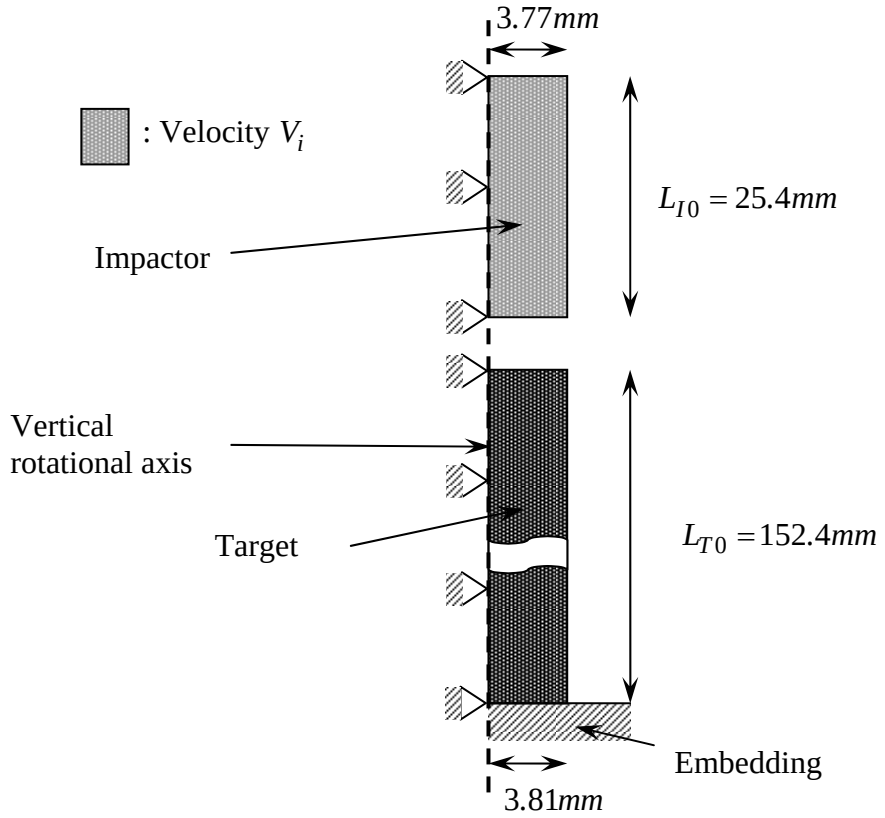

Figure 3. Schematic of the target and impactor for Taylor impact test (Rod-on-Rod).
Only half of the geometry is shown

These results show that the separation time period (opening of the gap at the cylinder base) is shorter using the physical approach than the phenomenological one (see also figure 4 and figure 5 for an impact at $260 m/s$). This gap appears after the radial release waves arrive at the centreline of the cylinder.

Table 6 summarises the numerical results of the projectile final diameter, at $2.5\mu s$, for two velocities values ($260 m/s$ and $365 m/s$).

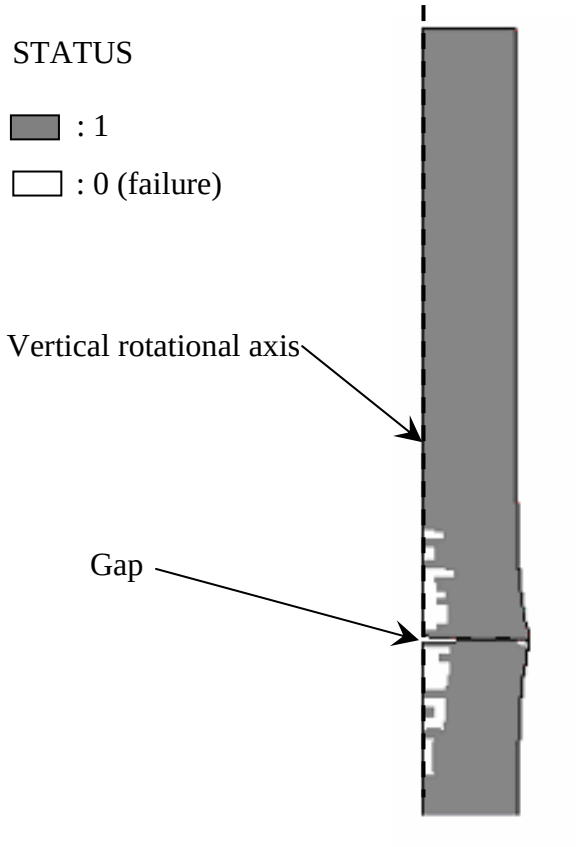

Figure 4. Calculated porosity contour for $V_i = 260 m/s$ considering Johnson-Cook approach at $3.75\mu s$

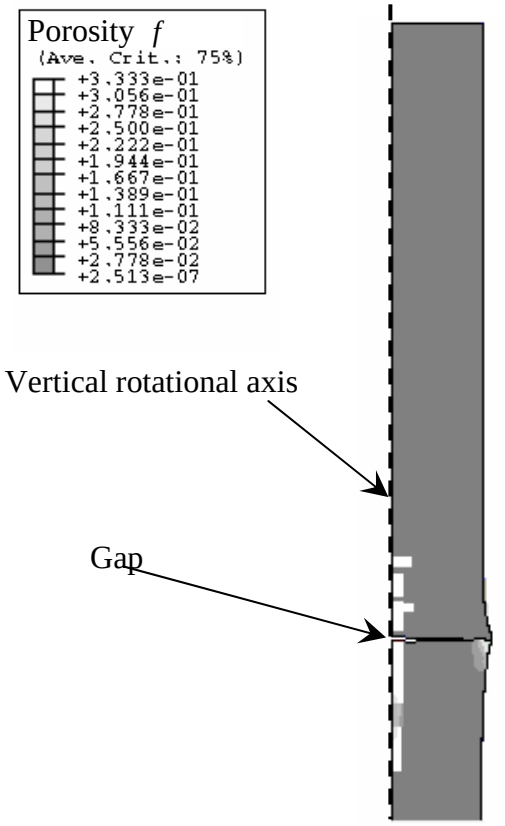

Figure 5. Porosity contour for $V_i = 260 m/s$ considering MTS+NAG approach at $2.5\mu s$

V_i [m/s]	Approach	Opening of the gap at the cylinder base
260	MTS+NAG approach	$2.5\mu s$ (figure 5)
	Johnson-Cook approach	$3.75\mu s$ (figure 6)
	experiment	Not known

Table 5. Comparison of the time of separation of the projectile at $260 m/s$ and according to various approaches

V_i [m/s]	Approach	Final diameter at the cylinder base of the projectile [mm]
260	MTS+NAG	10.3
	Johnson-Cook	11.03
365	MTS+NAG	12.2
	Johnson-Cook	12.18
	experiment	13.15

Table 6. Comparison of the final diameter of the projectile at various speeds at $2.5\mu s$ and according to various approaches

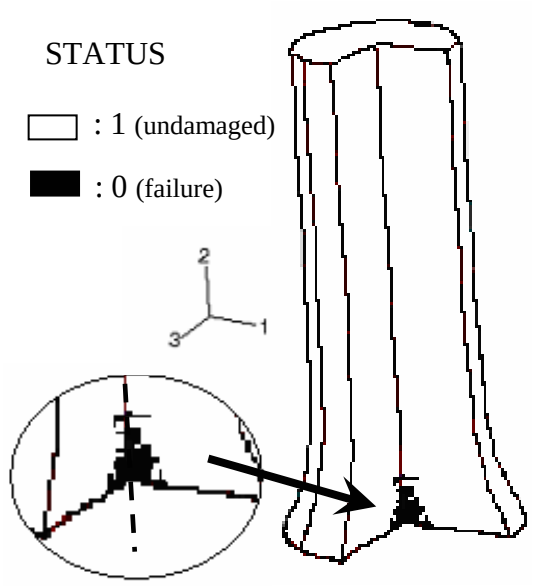

Figure 6. Porosity contour for $V_i = 260m/s$ considering Johnson-Cook approach at $3.75\mu s$

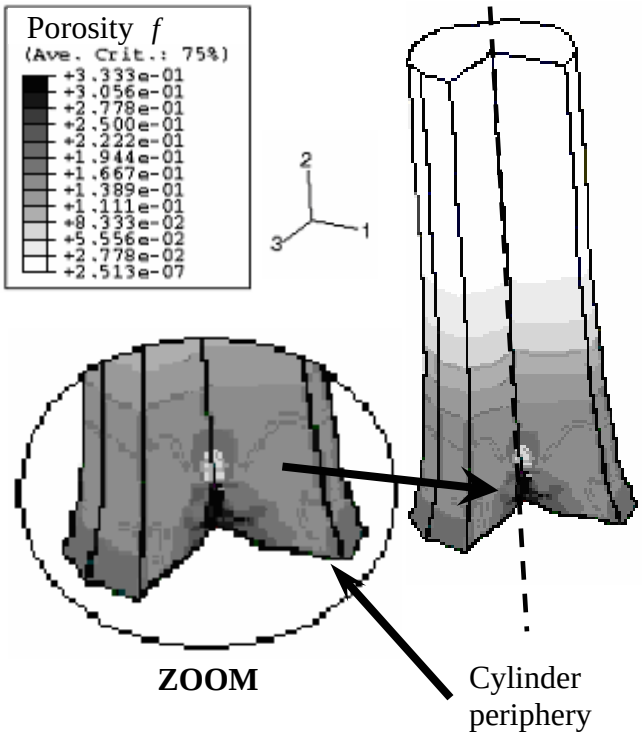

Figure 7. Porosity contour for $V_i = 260m/s$ considering MTS+NAG approach at $2.5\mu s$

For an impact velocity of $260m/s$, the simulation results using either the physical approach or the phenomenological approach show a similar failure zone along the cylinder axis (see figure 6 and figure 7). This porosity is due to the decompression wave when reaches the centerline of the target (decompression waves collide). It results in a region of tension in which the magnitude of the tensile wave is sufficiently high to produce a porous zone along the center line of the impacted

specimen. A similar result is observed in experiment [9]. This porosity is created by nucleation which is controlled by pressure. However, the physical approach results in a strong porosity zones on the cylinder periphery (see figure). These defects are created by nucleation which is controlled by the deformation.

For an impact velocity of $365m/s$, similar results for porosity are obtained in the degraded zone (along the axis) for Taylor impact test considering by the two approaches (Johnson-Cook approach and MTS+NAG approach) at $2.5\mu s$ (see Figure 8 and Figure 9). Moreover, the MTS+NAG approach predits porosity in the plastified zone, which is not predicted by the Johnson-Cook approach.

In Figure 10, the profile generated using the proposed (mechanistic) approach is in better agreement with the experimental data than the Johnson Cook model. The difference between our predicted profile and the experimental one, which is about 9 percent [see Table 6], can potentially be improved using a stronger damage-thermo-mechanical coupling.

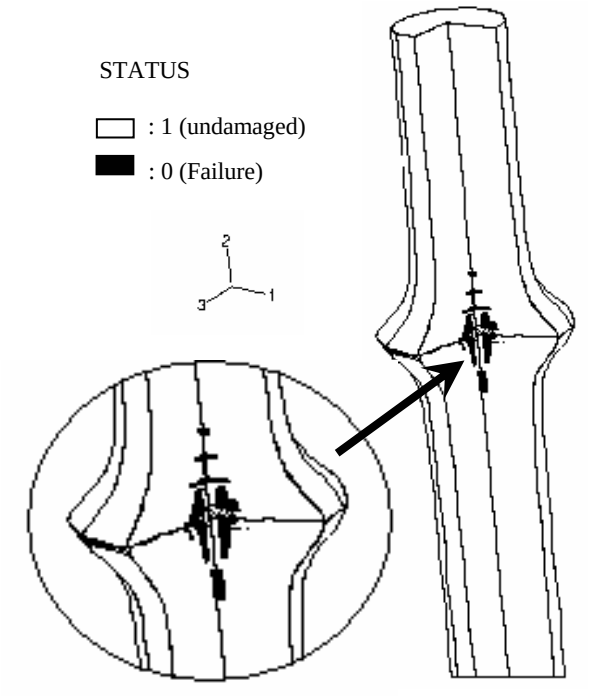

Figure 8. Porosity contour for $V_i = 365m/s$ considering Johnson-Cook approach at $2.5\mu s$.

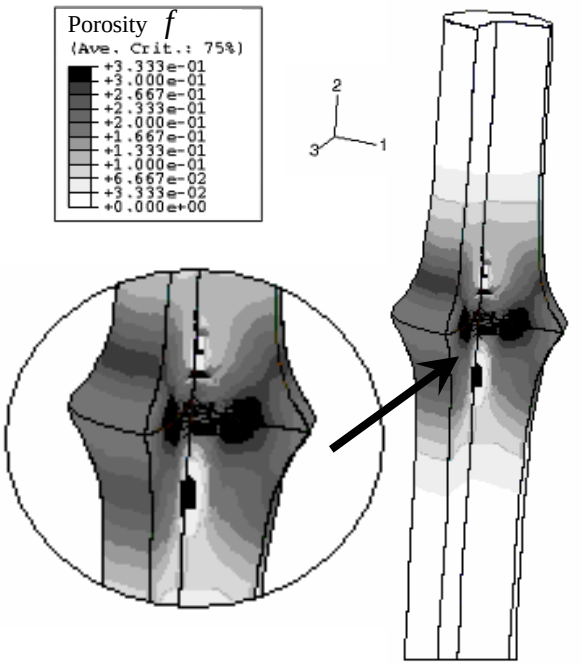

Figure 9. Porosity contour for $V_i = 365m/s$ considering MTS+NAG approach at $2.5\mu s$.

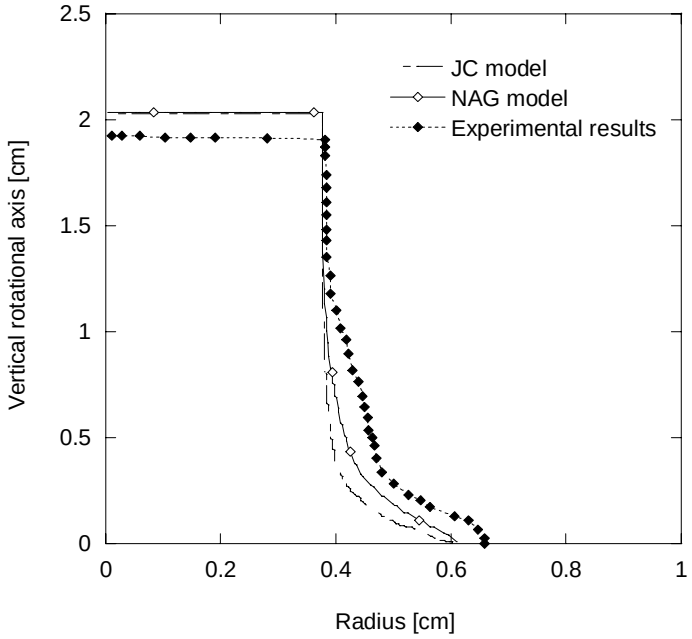

Figure 10. Comparison of experimental and simulated final cylinder profiles for the impact velocity of $365 m/s$

5. Conclusion

A computational modeling of Taylor impact on OFHC copper rods are carried out for two impact velocities ($260 m/s$ and $365 m/s$), using a physical approach (MTS+NAG models) as well as a phenomenological approach (Johnson-Cook approach). Similar qualitative results for porosity are obtained (for the two velocities) in the degraded zone (along the axis) for Taylor impact test by both approaches. In contrast to the phenomenological approach, our mechanistic approach results in a stronger porosity zone on the cylinder periphery. For an impact velocity of $365 m/s$, the profile generated using the proposed (mechanistic) approach is in better agreement with the experimental data than the Johnson Cook type approach. However, some differences between the predicted profiles and the experimental data still remain, and the results can potentially be improved using a strong thermo-mechanical coupling. Nonetheless, the Johnson-Cook approaches (for viscoplasticity and damage) implemented in standard Abaqus/Explicit can not be used with a strong thermo-mechanical coupling. In addition, this phenomenological approach does not predict damage evolution.

References

[1] Taylor G.I., The use of flat-ended projectiles for determining dynamic yield stress. I: theoretical considerations, Proc. R. Soc. Lond. A 1948; 194:289-299.

[2] Whiffen A. C., The use of flat-ended projectiles for determining dynamic yield stress. II: test on various metallic materials, Proc. R. Soc. Lond. A 1948; 194:300-322.

[3] Carrington W.E. and Gayler M.L.V., The use of flat-ended projectiles for determining dynamic yield stress. III: changes in microstructure caused by deformation under impact at high-striking velocities, Proc. R. Soc. Lond. A 1948; 194:323-331
[4] Johnson G.R., Cook W.H, A constitutive model and data for metals subjected to large strains, high strain rates and high temperatures, Proc. 7th Int. Symp. on ballistics 1983; The Hague, Netherlands, p. 541.
[5] Zerilli F.J. and Armstrong R.W., Dislocation-mechanics-based constitutive relations for dynamics calculations, J. Appl. Phys. 1987, 61(5):1816-1825.
[6] Johnson G.R. and Holmquist T.J., Evaluation of Cylinder-impact Test Data for constitutive Models Constants, J. Appl. Phys. 1988, 64:3901-3910.
[7] Pazienza G., Pezzica G. and Vignolo G.M., Determination of the Armstron-Zerilli Constitutive Model for AISI 316 H Stainless Steel and Application to cylinder Impact Tests, 7th Dymat Technical Conf., Saint-Louis 1992.
[8] Allen D.J., Use of the Taylor Impact Test to determine Constant for materials strength models, thesis, University of Alabama, Tuscaloosa 1995.
[9] Addessio F.L., Johnson J.N. and Maudlin P.J, The effect of void growth on Taylor cylinder impact experiments, J.Appl. Phys 1993; 73(11):7289-7292.
[10] Maudlin P.J., Foster J.C. and Jones S.E., A continuum mechanics code analysis of steady plastic wave propagation in the Taylor test. Int. J. Engng. 1996; 19(3):231-256.
[11] Rule W., Jones S.E., A revised form for the Johnson-Cook strength model. Int. J. Impact Engng, 1998; 21(8):609-624.
|12] House J.W., Aref B., Foster Jr. and Gillis P.P., Film data reduction from Taylor impact tests, Journal of strain analysis 1999; 34(5):337-345.
[13] Wang B., Zhang J. and Lu G., Taylor impact test for ductile porous materials-Part2: experiments 2003; 28:499-511.
[14] Follansbee, P.S., Kocks, U. F., A Constitutive Description of the Deformation of Copper Based on the Use of the Mechanical Threshold Stress as an Internal State Variable. Acta metall. 1988; 36(1): 81-93.
[15] Molinari A. and Ravichandran G., Constitutive modeling of high-strain-rate deformation in metals based on the evolution of an effective microstructural length. *Mechanics of Materials, Volume 37, Issue 7, July 2005, Pages 737-752*
[16] Molinari A. and Mercier S., Micromechanical modelling of porous materials under dynamic loading, Journal of the mechanics and Physics of solids 2001; 49: 1497-1516.
[17] Klopp R. W., Clifton R. and Shawki T. G., Pressure shear impact and the dynamic viscoplastic response of metals 1985; 4: 375-385.
[18]. Hanim S. and Ahzi S., A unified approach for pressure and temperature effects in dynamic failure criteria. Int. J. Plast. 2001; 17: 1215-1244.
[19] Tuler and Butcher, A criterion for time dependence of dynamic fracture. Int. J. Fract. Mech. 1968; 4:431.
[20] Gilman J.J., Micromechanics of flow in solids, Mc Graw-Hill 1969, New York.
[21] Curran, D. R., Seaman, L. and Shockey, D.A., Dynamic Failure of Solids. Physics reports 1987; 5-6(147):253-388.
[22] Rajendran A. M., Dietenberger M. A. et Grove D. J., A void nucleation and growth based failure model for spallation. J. Appl. Phys. 1988; 65: 1521-1527.
[23] Campagne L., Daridon L., Ahzi S., A physically based model for dynamic failure in ductile metals, Mechanics of Materials 2005; in press.
[24] Abaqus/Explicit, User's Manual, Version 6.4, Hibbit, Karlsson & Sorensen, Inc 2004; 25.3.4
[25] Meyers, M. A., Dynamic behavior of materials, Ed. Wiley-Interscience 1994, p.128-146.
[26] Weertman J., Fatigue crack growth theory for ductile material, In Three Dimensional Constitutive Relations and Ductile Fracture, ed. Nemat-Nasser S., North-Holland Publishing Company 1981;111-122.

[27] Meyers, M. A., Dynamic behavior of materials, Ed. Wiley-Interscience 1994, p.179-180.
[28]. Meyers, M. A., Dynamic behavior of materials, Ed. Wiley-Interscience 1994, p.106.
[29] Campagne L., Modélisation et simulation de la viscoplasticité et de l'endommagement en grandes vitesses de déformation, Thèse PHD, IMFS, Université Louis Pasteur, Strabourg 2003 ; 201p.
[30] Poizat C., Campagne L. Daridon L., Ahzi S., Husson C. and Merle L., Modeling and simulation of thin sheet blanking using damage and rupture criteria, International Journal of Forming Processes 2005 ; 9(1) : in press.
[31] Zaoui, A., Pineau, A., François, D., Comportement mécanique des matériaux, Tome: Elasticité et Plasticité, Ed. Hermes 1991.
[32] Lemaitre J., A Course on Damage Mechanics. Springer, Second Edition 1991.
[33] Bonora N., A nonlinear CDM model for ductile fracture, Engineering Fracture Mechanics 1997; 58(1):11-28.
[34] Tanner, A.B., McGinty, R.D. and McDowell D.L., Modelling temperature and strain rate history effects in OFHC Cu. Int. J. of plasticity 1999; 15:575-603.